Journal of Applied Polymer Science

Effect of Surfactant on EG Dispersion in EVA and Thermal and Mechanical Properties of the System

Shale J. Sefadi,[1] Adriaan S. Luyt,[1] Jürgen Pionteck,[2]

[1]Department of Chemistry, University of the Free State (Qwaqwa Campus), Private Bag X13, Phuthaditjhaba 9866, South Africa
[2]Polymer Reactions and Blends, Leibniz-Institut für Polymerforschung Dresden e.V., Hohe Str. 6, 01069 Dresden, Germany
Correspondence to: A. S. Luyt (E-mail: LuytAS@qwa.ufs.ac.za)

ABSTRACT: The influence of expanded graphite (EG) and sodium dodecyl sulfate (SDS) modified EG on the structure, thermal stability, and mechanical properties of ethylene vinyl acetate (EVA) was investigated in this study. The EVA filled with EG platelets, with and without anionic SDS modification, was prepared by melt mixing using a Brabender Plastograph mixer. The extent of dispersion and morphology of the composites were characterized using scanning electron microscopy (SEM), optical microscopy (OM), and X-ray diffraction (XRD). The optical microscopy results show better distribution of the modified EG platelets in the EVA matrix, while the SEM results show an improved interfacial adhesion between the polymer and the SDS-EG particles. Both the EVA18 copolymer and the EG platelets have monoclinic phases, and both EG and SDS do not seem to have any influence on the melting and crystallization behavior of the EVA18. The addition of EG enhanced the thermal stability of EVA18, and this stabilizing influence was further improved when the EG was treated with SDS. All the tensile properties of EVA/EG improved after surface modification. The storage modulus of EVA generally increased with increasing both the unmodified EG and the SDS modified EG content. There was a shift in the T_g to higher temperatures with an increase in both the EG and modified EG content. The α-relaxation peak in the SDS modified EG curves was less intense than the β-relaxation peak, even for the untreated EG composites. © 2014 Wiley Periodicals, Inc. J. Appl. Polym. Sci. **2015**, *132*, 41352.

KEYWORDS: composites; degradation; mechanical properties; polyolefins; properties and characterization

Received 14 March 2014; accepted 31 July 2014
DOI: 10.1002/app.41352

INTRODUCTION

Conductive polymer nanocomposites have attracted considerable interest, which is the result of their potential application in batteries, light emitting devices, electromagnetic shields, antistatic coatings and electrode materials.[1–3] The incorporation of conducting fillers such as intercalated graphite, carbon black, or metal and ceramic oxide powders into a polymer matrix is a promising approach to prepare conductive polymer nanocomposites.[4–6] Expanded graphite (EG) was used instead of other conductive fillers in this study because of its high corrosion resistance, low density and low cost.[7,8] Furthermore, the platelet-like structures in a polymer matrix often cause remarkable improvement in the material properties compared to those of the pure polymer. The improvements include enhanced physical and mechanical properties, especially high tensile moduli, increased thermal stability, decreased gas permeability and flammability, improved solvent and UV resistance, and improved electrical properties.[9,10] The main reasons for these enhanced properties are the high aspect ratios and large surface areas of the expanded graphite (EG) particles.

Natural graphite flakes are abundantly available and highly conductive with an electrical conductivity of 10^4 S cm^{-1} at room temperature.[2,11] Graphite is an allotrope of carbon whose structure is a single planar sheet of sp^2-bonded carbon atoms that are densely packed in a unique layered crystal structure.[11,12] However, it is relatively difficult to intercalate organic polymers or molecules directly into the interlayer of the graphite to prepare conductive polymer/graphite nanocomposites, due to the incompatibility between the components. This setback can be overcome by physical or chemical modification of the graphite.[13,14] The better dispersion of EG in an EVA matrix was achieved by modifying the EG with the anionic surfactant sodium dodecyl sulfate (SDS) via sonication. This modification improved the hydrophilicity of the EG, which should improve the interaction between the EG and EVA. Several papers were published on conductive thermoplastic polymer nanocomposites reinforced with EG prepared by *in situ* polymerization or solution intercalation,[13–16] but very little has been published on the preparation of these composites using melt-blending intercalation. Krupa et al.[17] studied the mechanical properties and

morphology of composites based on an EVA copolymer mixed with EG. Their copolymer contained 14% vinyl acetate. They observed that both tensile modulus and stress at break increased with an increase in EG platelets, while the elongation at break noticeably decreased. George et al.[18] investigated EVA/EG nanocomposites prepared by solution intercalation. They used an EVA with 60% vinyl acetate. In their case the tensile strength and modulus increased significantly up to 4% EG, while the elongation at break showed little change. Kim et al.[19] compared EVA/EG systems prepared by solution and three different melt mixing methods. Their EVA contained 18 wt % vinyl acetate, which is the same as the sample we used in our investigation. Their results show little change in thermal stability with increasing EG content and very little was reported on changes in the mechanical properties. Tavman et al.[20] and Tlili et al.[21] both compared the electrical properties of EVA (with 14 wt % vinyl acetate) containing respectively EG and unexpanded graphite. George et al.[22] reported a comprehensive study on reinforcement of EVA by differently treated naturally occurring graphites. The nanocomposites were prepared by a solution-mixing method. They found that the modified graphites showed better dispersion in and interfacial adhesion to the EVA matrix, containing 60% vinyl acetate, than the unmodified graphite. Similarly, significant improvements in filler dispersion and thermal stability were observed by George and Bhowmick[23] in their investigation of EVA with 40% VA content filled with modified EG nanofiller, using solution mixing and sonication.

The EVA copolymer with 18 wt % VA content used in this article is the same as the one used in our previous work on EVA filled with empty fruit bunch fiber.[24] As far as we could establish there is no other published work where the thermal and mechanical properties of EVA blended with EG and with surfactant modified EG prepared through melt-mixing were compared. The aim of our study was to investigate the morphology and thermal stability, as well as tensile and thermomechanical properties, of EVA filled with EG, without and with anionic SDS modification. For this purpose the EVA composites were prepared via melt-blending.

EXPERIMENTAL

Materials

Expanded graphite, SIGRAFLEX Expandat, was provided by SGL Technologies GmbH, SGL Group. It has a conductivity of 40 S cm^{-1} (room temperature, 30 MPa, self-made 2-points conductivity tester, coupled with a DMM2000 Electrometer, Keithley Instruments), an apparent volume of ~400 cm^3 g^{-1}, and a specific surface area of 39.4 m^2 g^{-1} (77.4 K, N_2 atmosphere, Autosorb-1, Quantachrome). Ethylene vinyl acetate (EVA-460) was manufactured and supplied in granule form by DuPont Packaging and Industrial Polymers. EVA-460 contains 18 wt % of vinyl acetate (VA) and a BHT antioxidant thermal stabilizer. It has a melt flow index (MFI) (190°C/2.16 kg) of 2.5 g/10 min (ASTM D1238-ISO 1133), a melting temperature (T_m) of 88°C, a Vicat softening point of 64°C, and a density of 0.941 g cm^{-3}. The sodium lauryl sulfate known as sodium dodecyl sulfate (SDS) was supplied by SIGMA-ALDRICH. SDS is a white powder with an assay of ≥99.0% (GC), a melting temperature range of 204–207°C and a molar mass of 288.4 g mol^{-1}.

Methods

Preparation of Nanocomposites. About 4 g of SDS were dissolved in 5 L deionized water in a glass beaker, and 20 g of the expanded graphite was gradually added to the solution. About 500 mL suspensions were sonicated for 30 min, filtered, followed by washing with 100 mL distilled water to remove loosely absorbed SDS and dried in a vacuum oven at 50°C for 72 h. This modified EG, as well as the as received unmodified EG, were respectively mixed with EVA to prepare the nanocomposites. The EVA composites were prepared by melt mixing using a Brabender Plastograph 55 mL internal mixer. The mixing was done for 15 min at 60 rpm and a temperature of 100°C. The samples were melt-pressed at 100°C and 50 bar for 5 min into 100 mm × 100 mm × 2 mm square sheets by using a hot hydraulic press.

Characterization and Analysis. The effect of surfactant on the EG dispersion of the EVA/EG and EVA/SDS-EG composites were studied by optical microscopy using a CETI-Topic B microscope, Belgium, with polarized light at 40× magnification. The thickness of the samples measured by the standard gage IP54 electronic micrometer ranges between 0.13 and 0.18 mm.

SEM analyses were carried out in a TESCAN VEGA3 Superscan scanning electron microscope (Brno, Czech Republic). The samples were fractured at liquid nitrogen temperature and the fracture surfaces of the samples were coated with gold by a Cressington Sputter Coater for 30 s. Microscope settings of 285.5 nm probe size, 50 mA probe current, 0.1 nm lateral resolution, and 30 kV AC voltage were used.

The structures of EG, SDS-modified EG and the EVA18 composites were determined through XRD. A D8 Advance diffractometer (BRUKER AXS, Germany) with PSD Vantec-1 detectors and Cu Kα radiation ($\lambda = 1.5406$ Å), a tube voltage of 40 kV, a current of 40 mA and a V20 variable slit was used. The samples were scanned in locked coupled mode with 2θ ranges from 0° to 120° at 2θ increments of 0.5 s $step^{-1}$.

DSC analyses were carried out under nitrogen flow (20 mL min^{-1}) using a Perkin Elmer Pyris-1 differential scanning calorimeter (Waltham, MA). The instrument was calibrated using the onset temperatures of melting of indium and zinc standards, as well as the melting enthalpy of indium. The sample weights were in the range of 5–10 mg, and they were heated from 25 to 180°C at a heating rate of 10 °C min^{-1}. The cooling and second heating were performed under the same conditions. For all the samples, the onset and peak temperatures of melting and crystallization, as well as the melting and crystallization enthalpies, were determined from the second heating scan. The normalized enthalpies of melting and crystallization in Table I was determined according to eq. (1).

$$\Delta H_m^{Norm} = \frac{\Delta H_{m,EVA}}{w_{EVA}} \quad (1)$$

where $\Delta H_{m,EVA}$ is the experimentally observed melting enthalpy for the pure EVA, and ΔH_m^{Norm} is the calculated normalized

Table I. Melting and Crystallization Enthalpies of all the Investigated Samples

wt % EG	$T_{p,m}$ (°C)	T_c (°C)	ΔH_m (J g^{-1})	ΔH_m^{Norm} (J g^{-1})	χ_c (%)
No modification					
0	85.5 ± 0.5	64.8 ± 0.2	13.0 ± 2.9	13.0	4.5
2	85.4 ± 0.4	64.8 ± 0.2	12.1 ± 0.9	12.3	4.3
4	86.0 ± 0.4	64.5 ± 0.2	12.1 ± 0.8	12.6	4.4
6	85.3 ± 0.4	64.8 ± 0.3	11.0 ± 1.3	11.7	4.1
8	85.5 ± 0.3	64.5 ± 0.1	11.2 ± 1.5	12.2	4.2
10	85.4 ± 0.4	64.7 ± 0.3	9.1 ± 1.4	10.1	3.5
SDS modification					
2	86.2 ± 0.1	65.5 ± 0.2	13.9 ± 1.2	14.2	4.9
4	85.5 ± 0.2	65.6 ± 0.1	14.3 ± 2.0	14.9	5.2
6	85.6 ± 0.3	65.6 ± 0.1	14.3 ± 2.1	15.2	5.3
8	85.5 ± 0.3	65.7 ± 0.2	14.4 ± 2.1	15.7	5.5
10	85.6 ± 0.3	65.6 ± 0.2	14.1 ± 0.9	15.7	5.5

$T_{p,m}$ is the peak temperature of melting; T_c is the crystallization temperature; ΔH_m is the measured melting enthalpy; ΔH_m^{Norm} is the calculated melting enthalpy of EVA18 taking into account its mass fraction; χ_c is the percentage of crystallinity.

enthalpy of melting for an EVA weight fraction w_{EVA} in the composite. The degree of crystallinity χ_c was calculated according to eq. (2).

$$\chi_c = (\Delta H_m^{Norm}/\Delta H_m^o) \times 100\% \quad (2)$$

where ΔH_m^o is the specific enthalpy of melting for 100% crystalline PE. A value of 288 J g^{-1} was used in the calculations.[25–27]

Thermogravimetric analysis was done under flowing nitrogen (20 mL min^{-1}) using a Perkin Elmer TGA7 thermogravimetric analyser (Waltham, MA). The samples, weighing about 20 mg each, were heated from 30 to 600°C at a heating rate of 10°C min^{-1}.

The tensile properties were investigated using a Hounsfield H5KS tensile tester at a cross-head speed of 10 mm min^{-1} and a gauge length of 20 mm. The tensile modulus as well as stress and elongation at break of the samples were determined from the stress-strain curves. At least five specimens were tested for each sample and the mean values and standard deviations are reported.

The viscoelastic properties of the composites were studied in the bending mode using a Perkin Elmer Diamond DMA (Waltham, MA) over a temperature range of −90 to +90°C at a heating rate of 5°C min^{-1} and a frequency of 1 Hz.

RESULTS AND DISCUSSION

Optical Microscopy

Figure 1 shows the microscopic images of EVA reinforced with untreated and treated EG platelets. The EVA/EG system [Figure 1(a)] shows a poor distribution of the dispersed phase because of inhomogeneity of the sample and poor interfacial interaction between the two components. The particle size distribution of the dispersed phases in the matrix ranges between 0 and 220 μm for the untreated EG samples. In the case of the EVA/SDS-EG composites [Figure 1(b)], it seems that there is a better particle size distribution due to the sonication applied during EG treatment with SDS, and because of improved interaction between the EVA and EG as a result of SDS modification. In this case the particle size distribution ranges between 0 and 120 μm. Our optical microscopy results are comparable with those obtained by Seo et al.[28] who investigated polyethylene and its copolymers filled with functionalized graphene. They observed large black functionalized graphene sheet aggregates that were coarsely dispersed in the polymer and a decrease in transparency when the graphenes were stacked into multilayers or agglomerated. Improved compatibility between the functionalized graphene sheets and the PE copolymers gave rise to a finer dispersion and better transparency.

Scanning Electron Microscopy (SEM)

Figure 2 shows the SEM micrographs of EG and SDS-EG at different magnifications. Figure 2(a) shows that EG has a wormlike structure about 500-μm long and consisting of loosely packed platelets with an interparticle porous character and a low bulk density. In Figure 2(b), the morphology of the sonicated SDS-EG seems to be similar to that of the crumpled paper. At higher magnification [Figure 2(d)], one can clearly see that the SDS has attached to the surface of EG, separating the EG layers. At higher magnification [Figure 2(c)] it is observed that EG has a structure of parallel sheets that collapse and deform randomly. This figure shows a network-like structure with many pores of different sizes, ranging from nanoscale to microscale. This observation is similar to the results reported by a number of other researchers[3,11,13,16,27–31] on the thickness of the EG sheets. Thus, the galleries between the EG sheets and the pores in the EG network provide a larger interlayer space and can readily be penetrated by the molten polymer. This finally results in a breaking up of the wormlike EG structure into dispersed platelets under melt mixing conditions.

The SEM micrographs of the fracture surfaces of the EVA composites filled with 2 and 6 wt % EG or SDS modified EG are

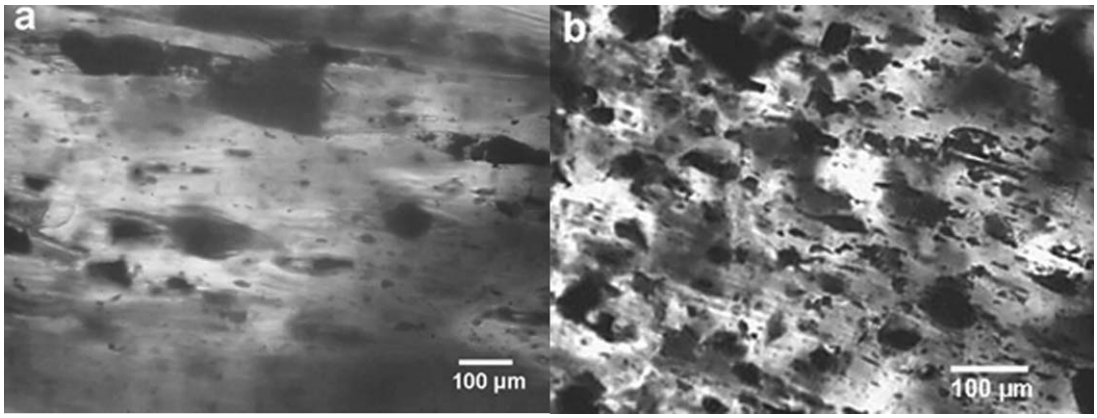

Figure 1. Microscopic images of the (a) 98/2 w/w EVA/EG and (b) 98/2 w/w EVA/SDS-EG composites.

shown in Figure 3. It can be seen, by comparing all the pictures, that the morphologies of the composites containing unmodified and modified EG are completely different. Figure 3(a,c) show that there are some particle agglomerations of EG present in the materials prepared without any dispersing agent. This is an indication that the EG sheets, like other types of nanoparticles, tend to agglomerate and are more difficult to disperse in the matrix by melt-blending than SDS-EG. During melt mixing, the shear force was insufficient to break down the EG agglomerates and to homogeneously disperse the graphite platelets in the EVA. It should be pointed out that, as the EG loading increased, the EG agglomeration observably increased for the samples prepared without SDS-modification. The presence of SDS modification seems to have restricted the graphite agglomeration, which resulted in a much better dispersed system [Figure 3(b,d)]. This is due to the sonication which was effective in dispersing the EG sheets, and the surfactant treatment, which reduced the EG particle-particle attraction. The better or finer dispersion due to the treatment of surfactant also contributed towards the improved compatibility between the EVA and SDS-EG. This has also been observed in previous literature,[32,33] and was explained as the surfactant molecules serving as a link between the graphite and the polymer, providing hydrophobic interactions. They also separate the graphite sheets, as was seen in Figure 2 and discussed above, providing space for the polymer chains to penetrate into the expanded graphite. The structural features observed here are similar to those observed on polyurethane (TPU)/graphite nanoplatelets conductive nanocomposites prepared by solution intercalation.[29] They found that there was a better shear during sonication which helped the graphite nanoplatelets to disperse better in the TPU matrix. Kim et al.[19] found that EG at 5 and 12 wt % was well dispersed in their EVA matrix.

X-ray Diffraction (XRD)

Figure 4 shows the XRD spectra of the pure EVA copolymer and EG. EG has a weak and broad peak at $2\theta = 11.4^\circ$ and a noticeable signal at $2\theta = 26.1^\circ$, respectively matching the (001) and (002) planes. The weak and broad peak represents less crystalline segments of the expanded graphite, while the narrow peak is attributed to the diffraction of a highly crystalline phase of the EG layers at an interlamellar distance of 0.34 nm, which is similar to that observed by other authors.[10,14] The diffraction peaks of EG describes a hexagonal EG structure with a lattice constant of 0.3420 nm. The XRD perfectly matches the standard data available in the Joint Committee on Powder Diffraction Standards (JCPDS) database of the International Centre for Diffraction (JCPDS 01–0646, www.icdd.com). The EVA in Figure 4 shows three different diffraction peaks at $2\theta = 21.3^\circ$, 23.5°, and 36.3° that respectively correspond to the (110), (200), and (020) crystallographic planes. These diffraction peaks are associated with an orthorhombic crystalline phase. The broad halo below the first two diffraction peaks represents the scattering of the amorphous segments.[22,25]

The XRD spectra of the EVA18 composites with unmodified and SDS modified EG (Figure 5) show no change in the position of the basal diffraction peaks (110) at $2\theta = 21.3^\circ$. This indicates that the addition of unmodified and modified EG did not significantly change the crystalline structure of the EVA18 matrix. The peak at $2\theta = 26.6^\circ$ is related to EG, and it shows an increased intensity with increasing EG and SDS-EG content. The peak positions were only marginally influenced and there is no trend. It is therefore clear that the presence of both EG and SDS modified EG had little influence on the crystal structure of EVA. George et al.[22] found that the intensity of the EG characteristic peak was reduced in the EVA/4EG composite due to an increase in amorphousness of the EVA matrix. They also found that EVA did not change the structure of EG and hence its crystal structure was retained.

Differential Scanning Calorimetry (DSC)

Figure 6 illustrates the changes in crystallinity (which was calculated from the DSC melting enthalpies) of the investigated samples as function of filler content. The enthalpy of melting of polyethylene (PE) was used to calculate the degree of crystallinity of EVA since there is no data available on the enthalpy of 100% crystalline EVA, and since only the PE segments, that form the backbone of EVA, crystallize. The crystallinity of the samples containing unmodified EG shows a 20% decrease, while that of the samples containing SDS modified EG shows a 20% increase. This observation must be related to the extent of agglomeration and/or dispersion of the EG platelets in the polymer. The platelets can act as nucleation centers which should

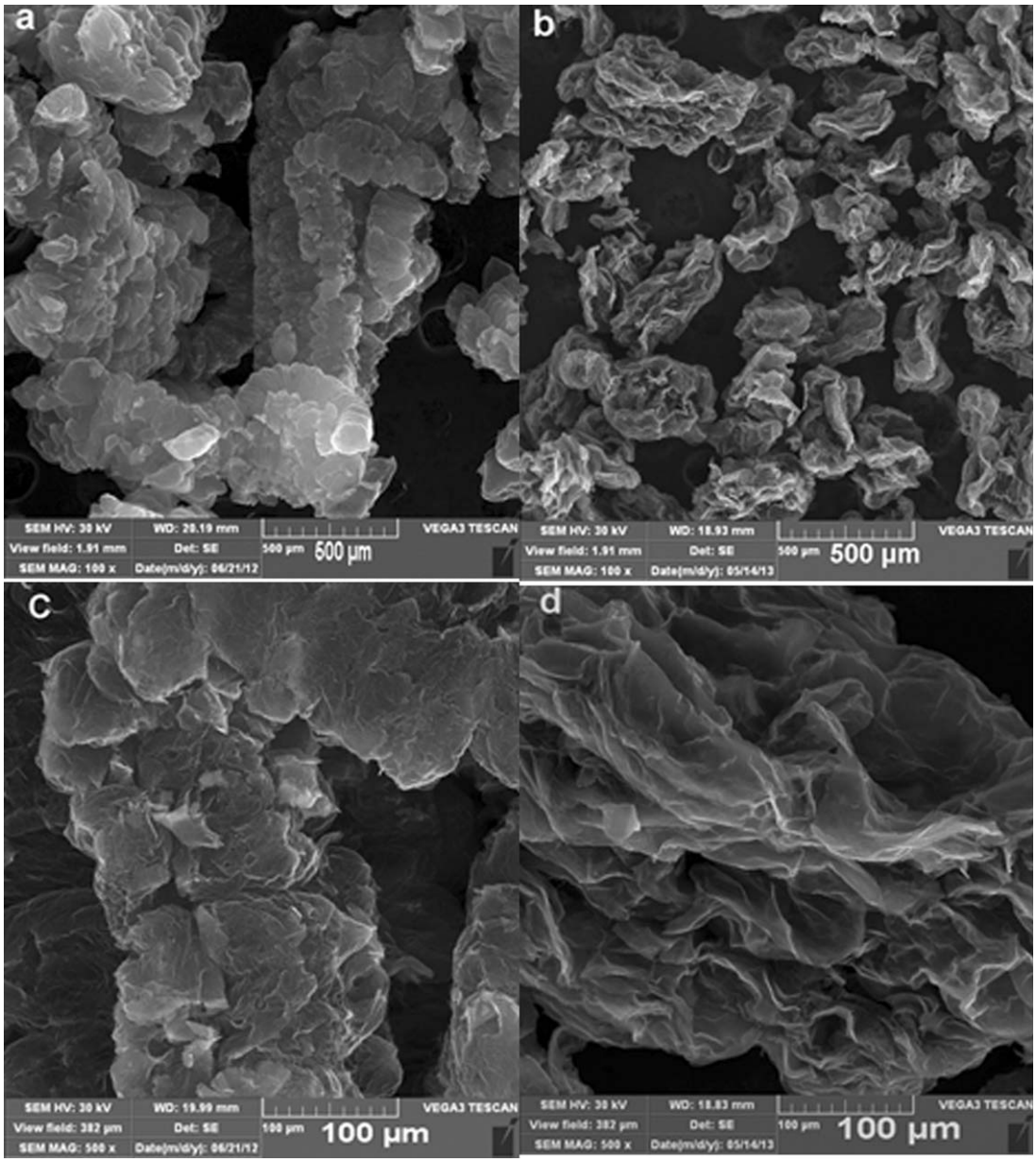

Figure 2. SEM micrographs of (a) EG (×100 magnification), (b) SDS-EG (×100 magnification), (c) EG (×500 magnification), and (d) SDS-EG (×500 magnification).

increase the crystallinity, or immobilize the polymer chains which should decrease the crystallinity. The nucleation effect seems to be more prevalent when the particles are smaller, as in the case of the SDS modified EG. Our previous study on the same EVA mixed with empty fruit bunch fiber[24] showed a smaller (10%) increase in EVA crystallinity, when mixed with the same amount of fiber, than the EVA mixed with SDS modified EG. The melting and crystallization temperatures as well as the melting and crystallization enthalpies of these samples are summarized in Table I. The melting and crystallization temperatures are the same within experimental error for all the samples.

Thermogravimetric Analysis (TGA)

The TGA curves of all the investigated samples are shown in Figures 7 and 8. It can be seen that the EG does not lose mass over the investigated temperature range of 0–850°C (Figure 7), confirming its thermal stability over this temperature range. The TGA plot of the SDS treated and washed EG shows a two-step degradation, which differs from that of untreated EG because of the SDS on its surface. The small mass loss of about 5% between 200 and 300°C corresponds to the evolution of degradation products of SDS. The mass loss of about 22% above 600°C can be ascribed to the decomposition of labile oxygen-containing functional groups present on the edges of the EG, which may be formed during sonication with SDS.[34–36] The TGA curve of SDS shows several mass loss steps in the temperature range 100–500°C. These are attributed to the dehydration of physically adsorbed water, followed by a decomposition process, the nature of which is not well defined. The SDS shows a residual amount of 23% after heating to 850°C.

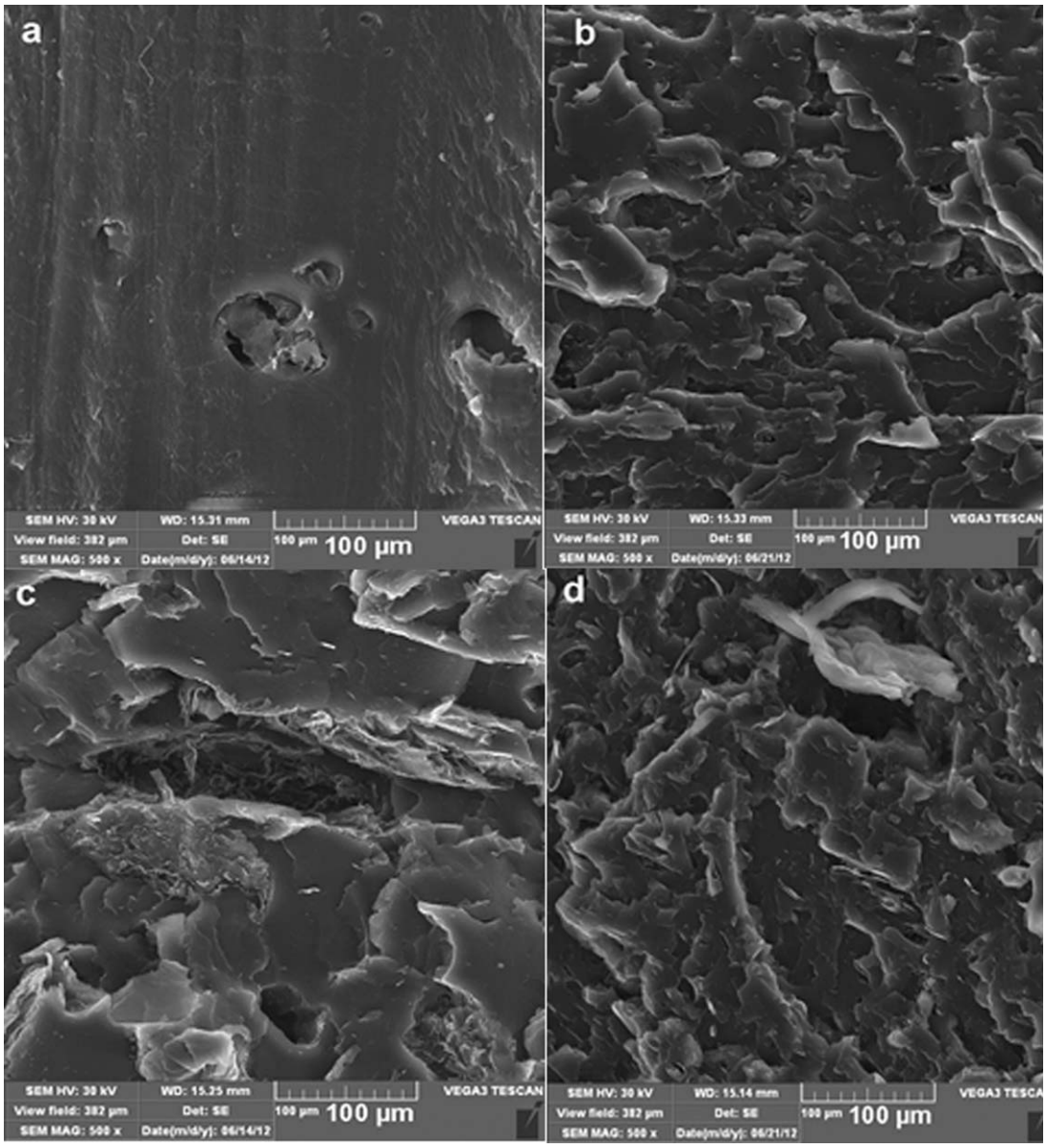

Figure 3. SEM micrographs of EVA18/expanded graphite nanocomposites: (a) 98/2 w/w EVA/EG; (b) 98/2 w/w EVA/SDS-EG; (c) 94/6 w/w EVA/EG; (d) 94/6 w/w EVA/SDS-EG.

Assuming that there is an additive degradation behavior of the EG-SDS sample, and taking the residuals of the EG, SDS, and EG-SDS at 550°C (99.3, 95.8, and 24.0%, respectively), one can calculate the SDS-content in EG-SDS to be 4.6 wt %.

The TGA curve of EVA (Figure 8) shows two degradation steps. The first step is attributed to deacetylation with β-elimination of the acetic acid and the formation of carbon–carbon double bonds along the polymer backbone. The second step is due to the main chain degradation and volatilization of the products formed through chain scission of the copolymer.[31,34–36] The decomposition of EVA and the volatilization of the decomposition products are completed at 500°C.

The EVA18/EG composites also show two degradation steps (Figure 8). Generally the incorporation of EG improved the thermal stability of EVA. The influence is not so obvious during the first degradation step. It seems that there is no stabilizing effect of EG on acetic acid elimination, but a strong effect on the main chain scission. It can be seen (Table II) that the T_{max} for the second degradation step of the EVA/EG samples increases with an increase in EG loading due to its strong stabilization effect, which is in line with previous observations on a similar system.[19] This was ascribed to the hindering effect of the EG layers on the diffusion of oxygen and volatile products through the composites.

The thermal stability of EVA was more significantly enhanced in the presence of SDS-EG than in the presence of unmodified EG (Figure 8). This is particularly clear when comparing the temperatures at the maximum rate of main chain scission of the

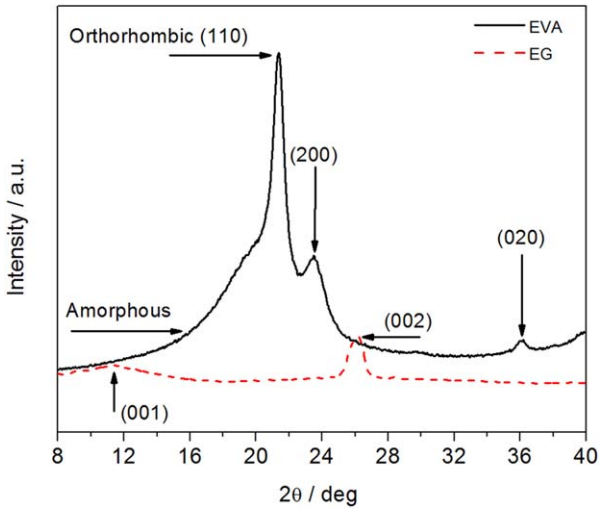

Figure 4. XRD diffractograms of EVA and unmodified EG. [Color figure can be viewed in the online issue, which is available at wileyonlinelibrary.com.]

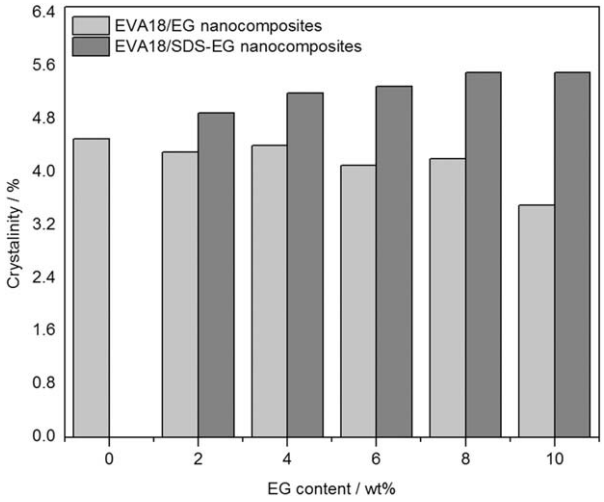

Figure 6. Crystallinity of the EVA18 composites with and without SDS as a function of EG content.

composites containing small amounts of filler (Table II). Only small amounts of SDS-EG already significantly improve the thermal stability of EVA. At 2 wt % SDS-EG, the T_{max} increased by 17°C, while in the case of unmodified EG the increase was only 3°C (Table II). The value of T_{max} continuously increases with increasing filler content in the case of EG, while this value only slightly increases with filler content in the case of SDS-EG, so much so that the T_{max} values are almost the same for the samples containing 10% EG and EG-SDS, respectively. Two parameters seem to play a role in determining the mass loss of EVA/EG and EVA-SDS-EG composites: strength of interaction between the polymer free radical chains and volatile degradation products and the filler, and the amount of filler that may interact with the free radical chains and volatile degradation products, and retard the degradation of the polymer and/or the diffusion of the volatile degradation products out of the polymer. It seems as if the strength of interaction is more dominant than the amount of filler, giving rise to the observed TGA results. For both EG and SDS-EG containing samples the residual amounts in Table II correlate well with the filler contents initially mixed into the polymer matrix, indicating that there is a good dispersion of the filler in EVA. This indicates the filler treatment only reduces the sizes of the filler particles, but does not have a significant influence on its dispersion in the polymer.

Tensile Properties

The stress and strain at break of pure EVA18 and its composites were determined from the stress-strain curves, some of which are shown in Figure 9. Both sets of samples exhibit considerable strain hardening, which decreases with increasing EG and SDS-

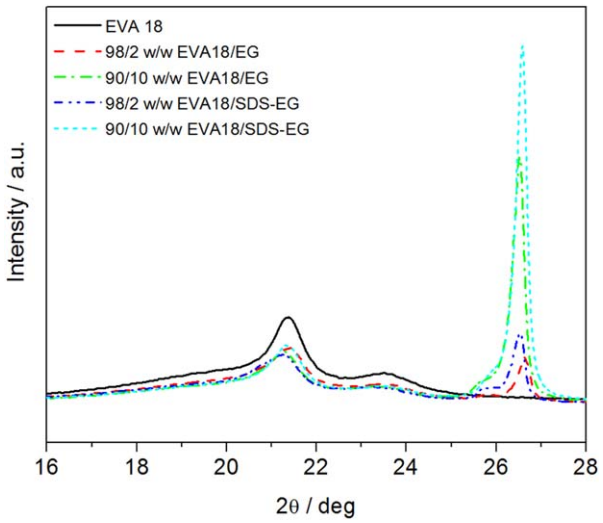

Figure 5. XRD spectra of the EVA 18 and its composites in the absence and presence of surfactant modification. [Color figure can be viewed in the online issue, which is available at wileyonlinelibrary.com.]

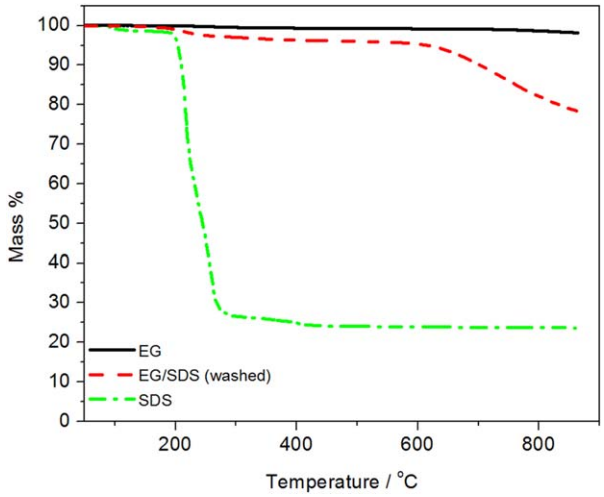

Figure 7. TGA curves of the EG, EG/SDS (washed) and pure SDS. [Color figure can be viewed in the online issue, which is available at wileyonlinelibrary.com.]

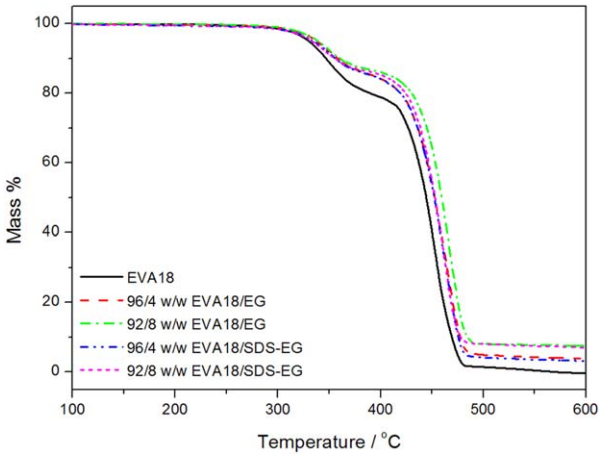

Figure 8. TGA curves of EVA18 and some of its composites. [Color figure can be viewed in the online issue, which is available at wileyonlinelibrary.com.]

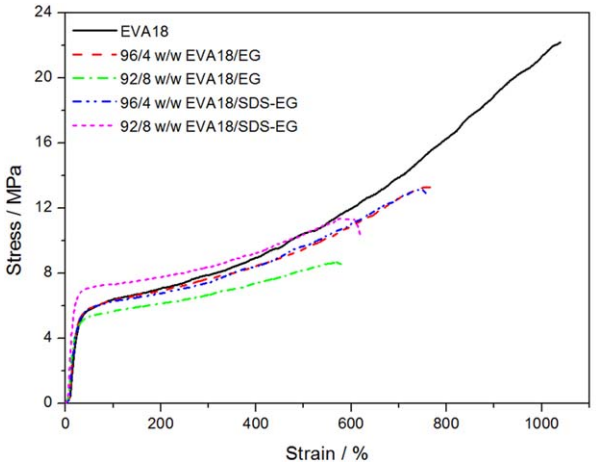

Figure 9. Stress–strain curves of the EVA18 and some of its composites. [Color figure can be viewed in the online issue, which is available at wileyonlinelibrary.com.]

EG content. There is also no clear yield point and no necking during stretching. The stress–strain curves show ductility which decreases with an increase in both EG and SDS-EG content. This suggests that the presence of EG inhibited the orientation of the chains in the amorphous regions of the polymer and the reorientation of the chains in the crystalline parts. This seems to be more prevalent in the case of the samples containing modified EG because of the finer dispersion and improved interaction with the polymer chains resulting in increased resistance against deformation.

Figure 10 shows the variation of stress at break, elongation at break and tensile modulus for EVA filled with EG and SDS-EG. For both fillers the tensile stress at break decreased significantly (from 22 Mpa for EVA to 8 MPa for EVA with 10 wt % EG), but the composites containing SDS-EG showed slightly higher stress at break values than the comparable composites with EG. Because of their higher extent of agglomeration, the EG particles in the EVA/EG composites are further from each other and the crazes formed during stretching more easily develop into cracks that lead to fracture at lower stresses. The EVA/SDS-EG systems have smaller and better dispersed EG particles that are closer to each other. It is therefore more difficult for cracks to develop, because a growing craze which started at one particle may terminate at another particle before it develops into a crack. More strain energy is therefore needed for crack development and growth, so that fracture occurs at higher stress values. In previous investigations a much smaller decrease in stress at break of 39% was observed for a 90/10 w/w EVA14/EG composite,[17] and a 36% increase in tensile strength for a 96/4 w/w EVA60/EG composite.[18]

Table II. TGA Results for all the Investigated Samples

wt % EG	$T_{10\%}$ (°C)	T_{max} (°C)	Weight % residue
No modification			
0	359.9	466.0	0
2	361.8	469.0	2.0
4	362.5	474.6	4.4
6	363.9	482.8	6.2
8	364.1	486.9	8.5
10	365.0	487.7	10.6
SDS modification			
2	362.9	482.9	2.3
4	364.9	484.0	4.1
6	366.4	485.0	5.7
8	367.0	485.2	8.3
10	367.7	486.1	9.9

$T_{10\%}$ and T_{max} are degradation temperatures at 10% mass loss and maximum or chain scission mass loss, respectively.

The elongation at break values show similar trends as the stress at break, and can be explained in the same way. Krupa et al.[17] observed a decrease in elongation at break of 90% for their 90/10 w/w EVA14/EG composite compared to our value of ~60% for both systems, while George et al.[18] observed a 32% decrease for their 92/8 w/w EVA60/EG composite.

The EVA/SDS-EG composites have modulus values that are about double those of the EVA/EG composites, and the modulus increases with increasing filler content for both types of composites. The modulus for the 90/10 w/w EVA/SDS-EG composite is 225% higher than that of the EVA, compared to 150 and 155% increases previously observed.[17,18] For both types of composites this increase is the result of the presence of the stiff EG platelets. The additional increase in the case of EVA/SDS-EG is due to the better dispersion of the SDS modified EG nanosheets and the better interfacial adhesion between the EG and EVA, leading to a restriction in chain mobility.

Dynamic Mechanical Analysis (DMA)

Some of the DMA results of EVA18 and its composites are presented in Figure 11. Table III shows the storage modulus values at −40 and 40°C for pure EVA and its composites. The storage

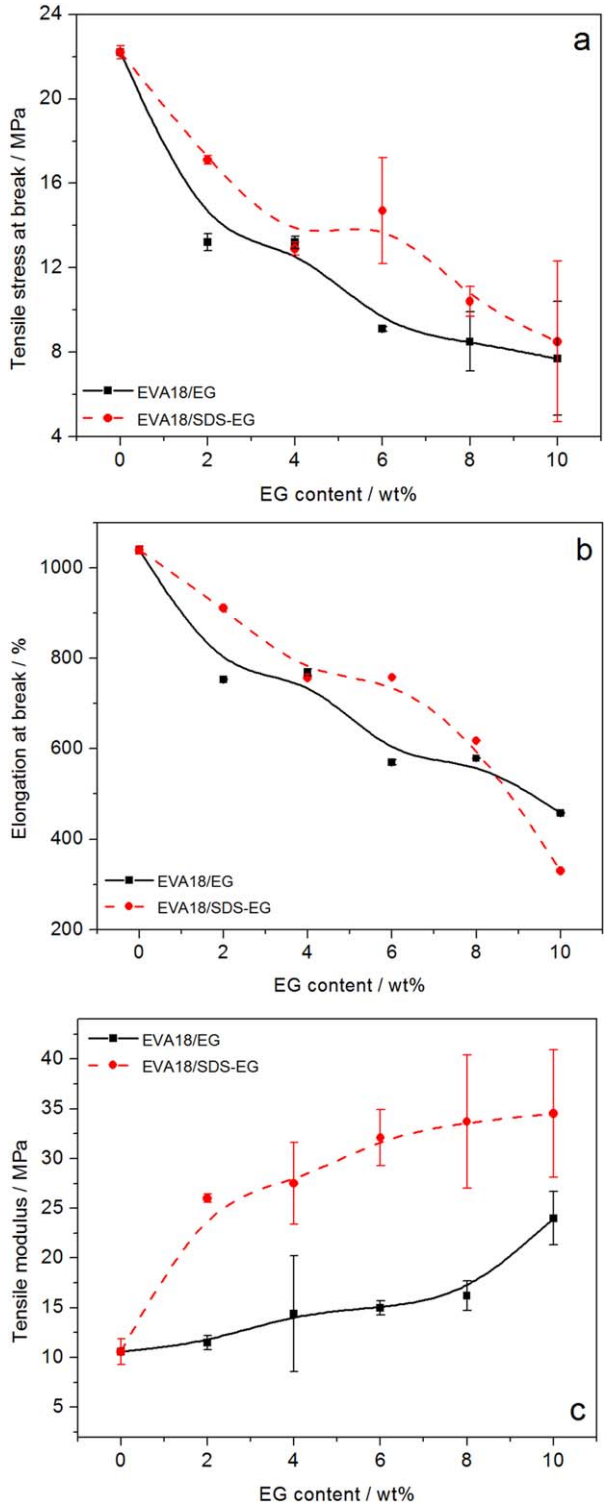

Figure 10. Variation of (a) stress at break, (b) elongation at break and (c) tensile modulus of EVA/EG and EVA/SDS-EG samples as a function of filler content. [Color figure can be viewed in the online issue, which is available at wileyonlinelibrary.com.]

modulus generally increases with increasing amount of both EG and SDS-EG in EVA18, which is due to the higher stiffness of the expanded graphite. Unlike our observations for tensile modulus discussed earlier, there were no significant differences in the storage modulus values of the samples containing modified and unmodified EG. There is also a big difference between the storage modulus and tensile modulus values, which shows that because of the dynamic nature of DMA, the amount of filler has a bigger influence on the observed elastic modulus than the interaction between the polymer and the filler. George et al.[18] observed a 16% increase in storage modulus at 20°C of their 92/8 w/w EVA60/EG composite over that of pure EVA60, while we observed an 83% increase for our 92/8 w/w EVA18/EG and 107% for our EVA18/SDS-EG.

The loss modulus curve of EVA18 (not included in article) shows a β-relaxation peak at −17°C, which is attributed to the glass transition of EVA. There are marginal differences between the peak temperatures of this transition between pure EVA18 and the composites, but since these differences are clearer from the tan δ curves, they will be discussed and explained below. There is little difference between the loss modulus curves for the EVA18/SDS-EG and the comparable EVA/EG composites.

The tan delta curve of EVA18 (Figure 11) shows two distinct relaxations, a β-relaxation at −6.2°C and an α-relaxation at 28°C. The β-relaxation is attributed to the motion of chain segments of three or four methylene (—CH_2) groups in the amorphous phase,[37,38] and is referred to as the glass transition (T_g). Below T_g the molecular chain segments are frozen in, the damping is low and a small amount of energy is stored for elastic deformations. In the rubbery region, the damping is high compared to the glassy state, because the molecular segments are free to move causing a decrease in stiffness, and excess energy is dissipated as heat. The α-relaxation is related to the motion of amorphous regions within the crystalline phase, which is probably the re-orientation of defect regions between the crystals.[38] The α-transition can also reflect the relaxation of flexible segments of the vinyl acetate (VA) groups present in the EVA copolymer chains. There is a shift in the T_g to higher

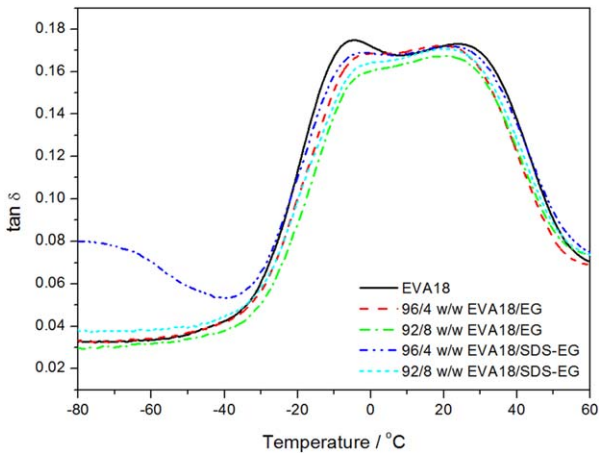

Figure 11. Dissipation factor as a function of temperature for pure EVA18 and the EVA18/EG composites in absence and presence of SDS modification. [Color figure can be viewed in the online issue, which is available at wileyonlinelibrary.com.]

Table III. Storage Modulus Values at −40 and 40°C for EVA Containing Untreated and Treated EG

	E′ of EVA/EG (Pa)		E′ of EVA/SDS-EG (Pa)	
Sample	T_{-40} (°C)	T_{40} (°C)	T_{-40} (°C)	T_{40} (°C)
Pure EVA	2.89×10^9	9.43×10^7	2.89×10^9	9.43×10^7
96/4 w/w EVA/filler	3.07×10^9	1.17×10^8	2.64×10^9	1.11×10^8
92/8 w/w EVA/filler	3.92×10^9	1.73×10^8	4.42×10^9	1.95×10^8

temperatures with an increase in EG content. This is indicative of reduced chain mobility in the amorphous regions of the polymer due to the interaction between EVA18 and EG, and is in line with previous observations.[18,24] The T_g of the SDS-EG containing composites shows similar increases with increasing filler content (Table IV). Therefore any improved interaction between the polymer and the filler had little influence on the glass transition temperature. The intensity of the β-relaxation peak decreased with increasing SDS-EG content, as in the case of the untreated EG, which indicates that the energy dissipation of the system decreased as a result of decreasing polymer chain mobility.

CONCLUSIONS

The effect of the EG and SDS modified-EG content on the structure and thermal stability of EVA18 nanocomposites was investigated. The distribution of EG was more homogeneous and uniform in the case of modified EG. The presence of EG (unmodified or modified) had little influence on the crystalline structure of EVA18, as well as on its melting and crystallization peak temperatures. The degree of crystallinity of EVA with SDS modified-EG was higher than that of EVA with unmodified EG, which is probably due to the smaller EG particles that acted as nucleation sites for EVA. The presence of EG in EVA18 increased its thermal stability, with SDS modification giving better results, even at low filler contents. The stress and elongation at break for all the EG containing EVA samples decreased markedly with increasing filler content, but the composites containing SDS treated EG gave better values. The tensile modulus values of EVA/SDS-EG were two times higher than those of the corresponding EVA/EG composites. There was a shift in the T_g to higher temperatures with an increase in both EG and modified EG content in the samples.

Table IV. Relaxation Temperatures for the EVA18, EVA18/EG, and the EVA18/SDS-EG Composites Determined from the tan δ Curves

	EVA/EG		EVA/SDS-EG	
Sample	β-relaxation temp. (°C)	α-relaxation temp. (°C)	β-relaxation temp. (°C)	α-relaxation temp. (°C)
Pure EVA	−6.2	27.8	-	-
96/4 w/w EVA/filler	−5.4	26.9	−5.3	26.5
92/8 w/w EVA/filler	−2.8	26.3	−2.4	25.9

ACKNOWLEDGMENTS

This work was financially supported by the National Research Foundation of South Africa and the International Bureau of the BMBF in Germany (project SUA 10/009).

REFERENCES

1. Wang, J.; Shi, Z.; Ge, Y.; Wang, Y.; Fan, J.; Yin, J. *Mater. Chem. Phys.* **2012**, *136*, 43.
2. Afanasov, I. M.; Morozov, V. A.; Kepman, A. V.; Ionov, S. G.; Sleeznev, A. N.; Van Tendeloo, G.; Avdeev, V. V. *Carbon* **2009**, *47*, 263.
3. Zhang, M.; Li, D.-J.; Wu, D.-F.; Yan, C.-H.; Lu, P.; Qiu, G.-M. *J. Appl. Polym. Sci.* **2008**, *108*, 1482.
4. Al-Hartomy, O. A.; Al-Salamy, F.; Al-Ghamdi, A. A.; Attieh Al-Ghamdi, A.; Abdel Daiem, A. M.; El-Tantawy, F. *J. Nanomater.* **2011**, *2011*, 1.
5. Shen, J.-W.; Chen, X.-M.; Huang, W.-Y. *J. Appl. Polym. Sci.* **2003**, *88*, 1864.
6. Kim, S.; Seo, J.; Drzal, L.T. *Compos. A* **2010**, *41*, 581.
7. Kalaitzidou, K.; Fukushima, H.; Drzal, L. T. *Compos. Sci. Technol.* **2007**, *67*, 2045.
8. Rath, T.; Li, Y. *Compos. A* **2011**, *42*, 1995.
9. Tsai, K.-C.; Kuan, H.-C.; Chou, H.-W.; Kuan, C.-F.; Chen, C.-H.; Chiang, C.-L. *J. Polym. Res.* **2011**, *18*, 483.
10. Yasmin, A.; Luo, J.-J.; Daniel, I. M. *Compos. Sci. Technol.* **2006**, *66*, 1179.
11. Dhakate, S. R.; Sharma, S.; Borah, M.; Mathur, R. B.; Dhami, T. L. *Int. J. Hydrogen Energy* **2008**, *33*, 7146.
12. Mo, Z.; Sun, Y.; Chen, H.; Zhang, P.; Zuo, D.; Li, Y.; Li, H. *Polymer* **2005**, *46*, 12670.
13. Chen, Q.; Wu, C.; Weng, W.; Wu, D.; Yan, W. *Polymer* **2003**, *44*, 1781.
14. Yuan, X. Y.; Zou, L. L.; Liao, C. C.; Dai, J. W. *eXPRESS Polym. Lett.* **2012**, *10*, 847.
15. Tantis, I.; Psarras, G. C.; Tasis, D. *eXPRESS Polym. Lett.* **2012**, *4*, 283.
16. Chen, G.-H.; Wu, D.-J.; Weng, W.-G.; He, B.; Yan, W.-L. *Polym. Int.* **2001**, *50*, 980.
17. Krupa, I.; Cecen, V.; Boudenne, A.; Križanová, Z.; Vávra, I.; Srnánek, R.; Radnóczi, G. *Polym. Plast. Technol. Eng.* **2012**, *51*, 1388.
18. George, J. J.; Bhowmick, A. K. *J. Mater. Sci.* **2008**, *43*, 702.
19. Kim, S.; Drzal, L. T. *J. Adhes. Sci. Technol.* **2009**, *23*, 1623.

20. Tavman, I. H.; Turgut, A.; Da Fonseca, H. M.; Orlande, H. R. B.; Cotta, R. M.; Magalhaes, M. *Int. J. Thermophys.* **2013**, *34*, 2297.

21. Tlili, R.; Boundenne, A.; Cecen, V.; Ibos, L.; Krupa, I.; Candau, Y. *Int. J. Thermophys.* **2010**, *31*, 936.

22. George, J. J.; Bandyopadhyay, A.; Bhowmick, A. K. *J. Appl. Polym. Sci.* **2008**, *108*, 1603.

23. George, J. J.; Bhowmick, A. K. *Nanoscale Res. Lett.* **2009**, *4*, 655.

24. Sefadi, J. S.; Luyt, A. S. J. *Thermoplast. Compos. Mater.* **2012**, *25*, 895.

25. Jing, J.; Chen, S.; Zhang, J. *J. Polym. Res.* **2010**, *17*, 827.

26. Chen, S.; Zhang, J.; Sun, J. *J. Appl. Polym. Sci.* **2009**, *114*, 3110.

27. Kim, S. R.; Poostforush, M.; Kim, J. H.; Lee, S. G. *eXPRESS Polym. Lett.* **2012**, *6*, 476.

28. Seo, H. M.; Park, J. H.; Dao, T. D.; Jeong, H. M. *J. Nanomater.* **2013**, *2013*, Article 805201.

29. Quan, H.; Zhang, B.-Q.; Zhao, Q.; Yuen, R. K. K.; Li, R. K. Y. *Compos. A* **2009**, *40*, 1506.

30. Liu, D.; Purewal, J. J.; Yang, J.; Sudik, A.; Maurer, S.; Maurer, U.; Mueller, U.; Ni, J.; Siegel, D. J. *Int. J. Hydrogen Energy* **2012**, *37*, 6109.

31. Weng, W.-G.; Chen, G.-H.; Wu, D.-J.; Yan, W.-L. *Compos. Interfac.* **2004**, *2*, 131.

32. Paruchuri, V. K.; Nalaskowski, J.; Shah, D. O.; Miller, J. D. *Colloids Surf.* **2006**, *272*, 157.

33. Cheng, H. K. F.; Pan, Y.; Sahoo, N. G.; Chong, K.; Li, L.; Chan, S. H.; Zhao, J. *J. Appl. Polym. Sci.* **2012**, *124*, 1117.

34. Smith, L. A.; Hammond, R. B.; Roberts, K. J.; Machin, D.; Mcleod, G. *J. Mol. Struct.* **2000**, *554*, 173.

35. Cheng, S.; Chen, X.; Hsuan, Y. G.; Li, C. Y. *Macromolecules* **2012**, *45*, 993.

36. Zhang, C.; Tjiu, W. W.; Fan, W.; Huang, S.; Liu, T. *J. Mater. Chem.* **2012**, *22*, 11748.

37. Grigoryva, O.; Fainleib, A.; Starostenko, O.; Tolstov, A.; Brostow, W. *Polym. Int.* **2004**, *53*, 1693.

38. John, B.; Varughese, K. T.; Oommen, Z.; Pötschke, P.; Thomas, S. *J. Appl. Polym. Sci.* **2003**, *87*, 2083.